FRANCIELE BRAGA MACHADO TULLIO
LUCIO MAURO BRAGA MACHADO
(ORGANIZADORES)

AMPLIAÇÃO E APROFUNDAMENTO DE CONHECIMENTOS NAS ÁREAS DAS ENGENHARIAS

Atena Editora
Ano 2020

FRANCIELE BRAGA MACHADO TULLIO
LUCIO MAURO BRAGA MACHADO
(ORGANIZADORES)

AMPLIAÇÃO E APROFUNDAMENTO DE CONHECIMENTOS NAS ÁREAS DAS ENGENHARIAS

Atena Editora
Ano 2020

Editora Chefe: Profª Drª Antonella Carvalho de Oliveira
Diagramação: Natália Sandrini de Azevedo
Edição de Arte: Lorena Prestes
Revisão: Os Autores

Atena Editora
Ano 2020

Atena Editora
Ano 2020

Dados Internacionais de Catalogação na Publicação (CIP)
(eDOC BRASIL, Belo Horizonte/MG)

A526 Ampliação e aprofundamento de conhecimentos nas áreas das engenharias [recurso eletrônico] / Organizadores Franciele Braga Machado Tullio, Lucio Mauro Braga Machado. – Ponta Grossa, PR: Atena, 2020.

Formato: PDF
Requisitos de sistema: Adobe Acrobat Reader
Modo de acesso: World Wide Web
Inclui bibliografia
ISBN 978-65-86002-74-4
DOI 10.22533/at.ed.744200804

1. Engenharia – Pesquisa – Brasil. 2. Inovações tecnológicas. 3. Tecnologia. I. Tullio, Franciele Braga Machado. II. Machado, Lucio Mauro Braga.

CDD 620

Elaborado por Maurício Amormino Júnior | CRB6/2422

Atena Editora
Ponta Grossa – Paraná - Brasil
www.atenaeditora.com.br

APRESENTAÇÃO

Em “Ampliação e Aprofundamento de Conhecimentos nas Áreas das Engenharias” vocês encontrarão dezenove capítulos que demonstram que as fronteiras nas engenharias continuam sendo ampliadas.

A engenharia aeroespacial brasileira vem realizando muitos estudos para a melhoria nos processos de construção de satélites e temos nesta obra quatro capítulos demonstrando isso.

Na engenharia elétrica e na computação temos quatro capítulos demonstrando empenho no aprofundamento de pesquisas envolvendo temas atuais.

A engenharia de materiais e a engenharia química trazem quatro capítulos com pesquisas na produção de novos materiais e produção de medicamentos.

Pesquisas na engenharia de produção temos três capítulos que demonstram o empenho na análise de qualidade da produção industrial.

Os demais capítulos apresentam boas pesquisas em engenharia civil, engenharia mecânica e engenharia agrícola.

Boa leitura!

Franciele Braga Machado Tullio

Lucio Mauro Braga Machado

SUMÁRIO

CAPÍTULO 12

THIN PLATE SPLINE INTERPOLATION METHOD APPLICATION TO PREDICT THE SUNFLOWER OIL INCORPORATION IN POLY (ACRYLIC ACID)-STARCH FILMS

Data de aceite: 27/03/2020

Talita Goulart da Silva
Departamento de Engenharia Química/Instituto de Tecnologia - Universidade Federal Rural do Rio de Janeiro, Seropédica, RJ, Brazil
tgoulart11@gmail.com

Débora Baptista Pereira
Departamento de Engenharia Química/Instituto de Tecnologia - Universidade Federal Rural do Rio de Janeiro, Seropédica, RJ, Brazil

Vinícius Guedes Gobbi
Departamento de Engenharia Química/Instituto de Tecnologia - Universidade Federal Rural do Rio de Janeiro, Seropédica, RJ, Brazil

Layla Ferraz Aquino
Departamento de Engenharia Química/Instituto de Tecnologia - Universidade Federal Rural do Rio de Janeiro, Seropédica, RJ, Brazil

Thassio Brandão Cubiça
Departamento de Engenharia Química/Instituto de Tecnologia - Universidade Federal Rural do Rio de Janeiro, Seropédica, RJ, Brazil

Matheus Santos Cunha
Departamento de Engenharia Química/Instituto de Tecnologia - Universidade Federal Rural do Rio de Janeiro, Seropédica, RJ, Brazil

Tiago dos Santos Mendonça
Departamento de Física Teórica/Instituto de Física A. D. Tavares - Universidade do Estado do Rio de Janeiro, Rio de Janeiro, RJ, Brazil

Sandra Cristina Dantas
Departamento de Engenharia Química/Instituto de Ciências Tecnológicas e Exatas - Universidade Federal do Triângulo Mineiro, Uberaba, MG, Brazil

Roberta Helena Mendonça
Departamento de Engenharia Química/Instituto de Tecnologia - Universidade Federal Rural do Rio de Janeiro, Seropédica, RJ, Brazil

ABSTRACT: Studies concerning the development of biomaterials have been performed in the last years. However, it is necessary to attempt to the transport phenomena, specifically absorption of fluids with healing properties, such as sunflower oil (SO), in the production of polymeric films applied to tissue regeneration. In this work, poly (acrylic acid)-starch films (PAA-S) were produced in different compositions (weight percent of starch ranging from 0 to 100 % wt) and characterized by scanning electron microscopy (SEM), Fourier transform infrared spectroscopy (FTIR) and atomic force microscopy (AFM). The PAA-S films were loaded with SO and the effect of the films composition on the SO absorption was evaluated. Thin plate spline interpolation method (TPSIM) was used to create a predictive data set, which were fitted by a polynomial to correlate swelling degree (S_w),

sample composition and time. The sine function was used to fit the mass variation data as a function of time, for the experimental and predicted compositions. PAA-S composition affects the morphology, as observed in the SEM and AFM analyses, and the SO absorption behavior. Oscillations in the S_w values were observed, probably, due to the heterogeneity of the films. The TPSIM was able to predict the films absorption capability and the sine function fitted properly the mass variation data ($R^2 > 0.99$).
KEYWORDS: modeling, transport phenomena, tissue engineering, biocompatible polymers, polymeric films.

INTRODUCTION

Wound healing is an important and complex process that involves a series of events, consisting of continuous and overlapping phases, such as hemostasis/inflammation phase, proliferation phase and remodeling phase for tissue reconstitution [1, 2]. In the tissue engineering interdisciplinary field, some technologies have been developed for deep wound healing and reconstruction of injured tissues, in which the use of biomaterials has been considered [3–5].

Poly (acrylic acid) (PAA), obtained from acrylic acid, is a synthetic and hydrophilic polymer [6]. In the medical field, it has been used as a gelling agent in medicines and in the synthesis of hydrogels for the development of drug delivery systems [7, 8]. Moreover, PAA based polymers are mostly used as controlled release tablets, oral suspensions and bioadhesives for oral and mucosal contact applications [8]. According to their biocompatibilities and functionalities, bioadhesives can be further divided into two categories, namely external bioadhesives and internal bioadhesives [9].

Starch is a natural polymer composed of anhydroglucose units, capable of forming two homopolymers, namely amylose and amylopectin. This material occurs in granule form in stems, tubers and seeds of different plants, such as rice, corn, potato and others [8, 10]. It has numerous applications, such as its use in the production of bags, mulch films, wrapping films, paper laminations, nets, cutlery, flower pots and boxes. This polymer also has potential for biomedical applications, including substrates for cell seeding, scaffolds for tissue engineering, bone replacement implants and drug delivery systems [10–15].

The bioadhesive polymeric films may be used as topical drug delivery systems, being capable of improving the pharmacotherapy and patient compliances [16]. The use of plant-derived products has increased over the years, especially for the treatment of wounds [17, 18]. The Dersani® oil, derived from the sunflower seeds, is composed of triglycerides of capric and caprylic acids, clarified sunflower oil (SO), lecithin, retinol palmitate, tocopherol acetate and alpha-tocopherol. The linoleic acid,

a fatty acid, present in the composition of SO, may alter the inflammatory response and improve the process of tissue restoration, and, due to this fact, it has been used in the treatment of wounds [19].

Attention has been done to the mathematical modeling of polymer behavior as, for example, polymer swelling, since this property is very important in drug delivery systems and in the incorporation of fluids into polymeric matrices. According to literature, sorption processes for polymer-solvent systems frequently do not conform to the behavior expected from the classical theory of diffusion [20].

Thin plate interpolation method (TPSIM) provides interpolated values of a real function and it is highly useful in many applications, such as thermal studies, medical researches, polymer characterizations and others [21–25]. This method, as a Generalized Additive Model (GAM), has some advantages, for example, there is no need of previous knowledge of the functional form of the data [24].

Interpolation may be used for making prediction [26] and may be a good alternative to predict the effect of materials composition and time in the fluid incorporation studies and the use of TPSIM in polymer swelling behavior has been studied by our research group [27] for polymeric systems as, for example, matrices of polyhydroxybutyrate and chitosan. In this work, it was produced poly (acrylic acid)-starch (PAA-S) films which were loaded with SO. In this context, swelling is an alternative for incorporating drugs into the biomaterials and, thus, the specific aims of this work were:

I. To evaluate the absorption of SO by PAA-S films (by the study of mass variation as a function of time – experimental data);

II. To apply TPSIM to predict the absorption data increasing the data set (by the generation of interpolated data based on the experimental values);

III. To apply a local model in the obtained data (experimental and interpolated data), in this work, it was opted for the selection of an equation that allows periodicity, thus, the sine function was adopted;

IV. To apply a polynomial fit (p55) to the interpolated data set, to create a surface that correlates SO absorption, time and composition.

EXPERIMENTAL

Materials

Corn starch (Unilever, Brazil) and PAA (Sigma-Aldrich) (Mv ~ 4,000,000) were used as raw materials in the production of films.

Methodology

To prepare the PAA-S films, corn starch and PAA powders were added to water and heated at 70 °C for 15 min. The resulting mixtures were placed into silicon molds and were taken to a microwave (Electrolux, Power 1620 W) for 7 minutes. The films were named according to the compositions: PAA (100 wt % PAA); PAA-S10 (90 wt % and 10 wt % starch); PAA-S20 (80 wt % and 20 wt % starch); PAA- S40 (60 wt % and 40 wt % starch); PAA-S70 (30 wt % and 70 wt % starch); PAA-S90 (10 wt % and 90 wt % starch); starch (100 wt % starch).

Scanning Electron Microscopy (SEM)

To analyze the effect of composition in the PAA-S films morphology, the films (PAA, PAA-S10, PAA-S20, PAA-S40, PAA-S70, PAA-S90 and Starch) were evaluated using a scanning electron microscope HITACHI, model TM3000 (Japan) at an acceleration voltage of 15 kV.

Fourier-transform infrared spectroscopy (FTIR)

A chemical analysis of the produced films was carried out using an Infrared Spectrometer Bruker, model Vertex 7 (EUA) under attenuated total reflectance (ATR) by recording measurements from 4500 to 500 cm–1.

Swelling Degree Analysis

To determine the PAA-S films swelling degree (SW), the samples were immersed in SO for 1 hour. The films mass variations were verified at intervals of five minutes. The swelling degree was calculated using Equation (1).

$$S_w = \left(\frac{W_t - W_0}{W_0}\right) x100 \quad (1)$$

Where W_t is the weight of the films at time t and W_0 is the initial weight.

Atomic force microscopy

AFM analysis was conducted on the atomic force microscope JPK Instruments, model Nanowizard (EUA). The films topography was analyzed in intermittent contact mode using silicon nitride needles (MikroMasch ™ NSC16) mounted on a rod with a spring constant of 40 N/m and a resonance frequency of 170 kHz. The films were fixed on double-sided tape and the AFM images were obtained in the air.

Thin plate spline interpolation method (TPSIM) and polynomial fitting

Thin plate spline interpolation method was used to predict the S_W behavior of PAA-S films and the relation Mi/M∞ (Equation (2)).

$$\frac{M_i}{M_\infty} = \frac{weight\ at\ t = i}{weight\ at\ t = \infty} \quad (2)$$

Where i ranges from 0 to ∞, with ∞ equal to 60 min.

That is, to estimate/predict values of oil incorporation that lies between known data points. The 3D data used were: S_W (obtained by Equation (1)), sample composition and time to predict the S_W values and, to predict the Mi/M∞, the data used were: Mi/M∞ (obtained by Equation 2), sample composition and time. TPSIM was applied: (i) using real mass variation data (obtained experimentally) and (ii) using predicted data while omitting the real mass variation data. The data obtained in (i) were compared with the data obtained in (ii). For this purpose, data from the samples PAA-S10, PAA-S20, PAA-S40, PAA-S70, and PAA-S90 were selected. The experimental values obtained for the 100% starch and 100% PAA films were maintained as boundary conditions, being part of the data set used in both (i) and (ii). The data generated in (i) and (ii) were compared and ANOVA was used to evaluate if there was a significant difference ($p < 0.05$). Although TPSIM provides 3D data, it was decided to plot the relation Mi/M∞ versus time for several concentrations (ranging from 1 to 100%, with intervals of approximately 2%), to compare the experimental data and the predicted data obtained by TPSIM. TPSIM was applied using the function thin plate spline on computational software Octave.

Polynomial fit p55 applied to the swelling degree data obtained by TPSIM

A polynomial fit p55, showed in Equation (3), was applied, simultaneously, to the experimental and the interpolated data, to obtain a 3D surface that correlates S_W, composition and time [27].

$$f(x,y) = \sum_{m=0}^{5}\sum_{n=0}^{5} p_{mn}\, x^m y^n \quad (3)$$

In this work, f(x,y) is the S_W, x is the matrices composition (represented by the starch amount in the sample) and y is the time. According to Equation (3) it is important to observe the following statements:

1. If n = 0 zero and m > 0, the term of the polynomial (pmn) only depends on the variable x (composition);
2. If m = 0 zero and n > 0, the term of the polynomial (pmn) only depends on the variable y (time);
3. If n > 0 and m > 0, the term of the polynomial (pmn) shows the interaction between the variables x and y.

Modeling based on the Mi/M∞ relation

There are number of kinetic models, which describe the overall mechanism of diffusion in polymeric matrices. Some empirical models may satisfactorily describe the experimental data based on theoretical considerations, such as the Power Law model [20]. In this work, due to the characteristics of the samples and to the curve behavior of Mi/M∞ versus time, it was opted for the selection of an equation that admits periodicity to fit the data. In this case, the sine function was applied (Equation (4)). It is worth mentioning that the interval, that includes the values of Mi/M∞, varies from 0 to 1, which facilitates the application of this function. Although TPSIM provides 3D data (Mi/M∞ relation, composition and time), it was decided to utilize a 2D fit for several concentrations (ranging from 1 to 100%, with intervals of approximately 2%), to establish a function capable of looking at all the selected curves, that is, the mass variation as a function of time. This 2D fit correlates for each composition, Mi/M∞ relation versus time. The Power law model was also applied; however, the function did not adjust properly to all curves (interpolated and experimental data), thus, the data obtained will not be presented in this paper.

$$y = \sum_{i=1}^{n} a_i \sin(b_i x + c_i) \tag{4}$$

Where a_i is the amplitude, b_i is the frequency, c_i is the phase constant for each sine wave term and n is the number of terms in the series, generally with $1 \leq n \leq 8$ and, in this work, it was used n = 4, because the obtained coefficients for n > 4 were not significative. This equation is closely related to the Fourier series. The main difference is that the sum of sines equation includes the phase constant, and does not include a constant (intercept) term.

RESULTS AND DISCUSSION

PAA-Starch (PAA-S) films were produced in different compositions utilizing a microwave. The resulting films were characterized chemically and morphologically.

To evaluate possible chemical interactions between PAA and starch, the starting materials and the films were analyzed by FTIR (Fig. 1 and Fig. 2) and the respective bands and assignments may be observed in Table 1.

The large band (Fig. 1) observed between 3000 and 3628 cm-1 is linked to the O-H stretching of the glyosidic group present in the molecules of starch. These characteristics peaks are in accordance with literature [28, 29]. The spectrum of pure PAA (Fig. 1) presented a wide band between 2900 and 3600 cm-1 and a band between 3100 and 2800 cm-1. These bands are related, respectively, to O-H stretching vibration of carbonyl groups and to CH2 and CH stretching vibration. The presence of remained water from the films production process, in the PAA films, may have affected the bands shape on the wavenumber ranging from 3500 to 2800 cm-1 [29]. The FTIR spectrum of PAA is also in accordance with literature [28–30].

Fig. 2 shows FTIR spectra of PAA-S films. The spectra show characteristics of both polymers, PAA and starch. However, it is important to note that in the spectra where the PAA concentration was higher (PAA-S10, PAA-S20, PAA-S40), PAA characteristic bands probably overlapped those attributed to starch. Similarly, it was observed, for PAA-S60, PAA-S70 and PAA-S90 samples, which contain more starch than PAA, that starch bands overlapped PAA bands.

The band at 2925 cm-1, characteristic of starch CH groups is present in the blends where the starch concentration is higher. In the case of the samples with higher PAA concentration, this band was overlapped. There was an increase in the characteristic peak of C = O bonds in the samples with the highest concentration of PAA. In the sample containing the highest starch concentration, it was possible to identify the profiles corresponding to C = O (1690 cm-1) interaction of PAA and OH (1640 cm-1) of starch, which was not possible in the other concentrations (PAA-S90, PAA-S70, PAA-S60), since these bands merged. Similar behavior was observed by Bin-Dahman et al. [29], that prepared PAA and corn starch blends by using solution mixing and casting method. They attributed this to the nature of interaction between PAA and starch via hydrogen bonding.

Fig. 3 shows SEM images of the following films: 100% PAA, PAA-S10, PAA-S20, PAA-S40, PAA-S70, PAA-S90 and 100% starch. It is possible to see that the films morphology was affected by composition (see the arrows in Fig. 3) and a heterogeneous surface was formed for the PAA-S10, PAA-S20, PAA-S40, PAA-S60, PAA-S70 and PAA-S90 samples, due, probably, to the partial miscibility of PAA and starch, as also observed by Bin-dahman et al. [29]. Similar result was observed by Bardajee et al. [28], where the morphology and composition of the optimized hydrogel were altered according to the different amounts of PAA and starch. This behavior was also observed in the synthesis of thin films of PAA hybrid nanocomposites with starch nanocomposites as packaging materials reported by Sethy et al. [31], where

starch flaxes were accommodated in the PAA network and micropores were noticed on the surface of the copolymer matrix.

The SEM images (Fig. 3) suggest that a heterogeneous surface was formed. This result is more clearly observed for the PAA-S20 and PAA-S60 samples. Therefore, AFM analysis of PAA-S20 was performed and the result is shown in Fig. 4. The AFM images corroborate the SEM results, since it is possible to see in the same sample (PAA-S20) regions with different morphologies. Rounded and elongated structures inserted in a smoothed surface can be observed, probably due to the interactions between PAA and starch.

Literature fails to provide papers where AFM analysis is used to evaluate films made of PAA and starch. However, it was found papers that used AFM to analyze starch-based films and PAA-based films separately, as in the work of Fazeli et al. [32], which starch-based composite films reinforced by cellulose nanofibers were prepared and characterized. It was observed that the surface roughness of the reinforced film was lower when compared to the pure film, showing that the addition of the cellulose nanofibers altered the morphology of the starch-based film. A similar result was observed by Vebber et al. [33] in the production of PAA, poly (allylamine hydrochloride) and titanium dioxide self-thinning films for the photo oxidation of ibuprofen, where changes in morphology were observed in the topography obtained by AFM.

The 100% PAA, PAA-S10, PAA-S20, PAA-S40, PAA-S60, PAA-S70, PAA-S90 and 100% starch samples were immersed in SO and the S_w values were obtained by Equation (1). Thus, in order to increase the data set, TPSIM was applied. Fig. 5 shows a data set composed of S_w values (obtained experimentally) and predicted S_w values (obtained by interpolation). It was observed that the S_w values (Fig. 5) fluctuate according to the composition of the films. In addition, it was also observed, for all studied compositions, that S_w oscillations occurred as a function of time.

The morphology analysis of PAA-S films as well as the FTIR study showed that the films present characteristics of pure materials and these are strongly influenced by the concentration. According to the FTIR analyses, there is remained water in the films with greater amount of PAA. Nevertheless, PAA is more polar than starch, which may explain the fact that samples containing more starch absorbed more oil. In Fig. 5, it is possible to understand that there is a more pronounced inflection in the central region of the image (the absorption tends to be at a minimum) and this region is further from the borders, which correspond to the pure materials. This inflection may be correlated to the fact that PAA and starch swelling differ from each other, which may promote the compression of the starch phase and the PAA-S phase, characterized by the negative mass variation, in comparison with the studied interval, although swelling occurs at time zero. The highest absorption

results for SO were obtained by the samples with the highest amount of starch in its composition, however, the data obtained also show that there was an oscillation in the S_w values when comparing samples with different compositions, probably due to the heterogeneities present in the samples, as observed in the SEM and AFM analyses (Fig. 3 and Fig. 4).

The polynomial fit (p55) (Equation (3)) was used to investigate the contribution of time (y) and composition (referred as the mass percentage of starch in the sample, x) in S_w values. In this polynomial, there is the contribution of concentration, time and also the interaction between these two variables. The coefficients obtained for this polynomial may be observed in Table 2 and they represent the fitted surface obtained for the swelling in SO (Fig. 6). It is possible to note in Fig. 6 and in Table 2 (based on the polynomial coefficients) that S_w is strongly related to composition and to the exposure time of samples to SO. It is important to clarify that not all of the polynomial terms were presented in Table 2, due to the fact that the omitted terms are practically null and do not significantly contribute to the final y value.

Bin-Dahman et al. [29] evaluated the S_w of PAA-S blends in water and found out that the higher the amount of PAA in the sample, the greater the S_w. A similar result was observed by Badajee et al. [28], since the S_w of PAA-S based films, developed in their work, increased with the increasing amount of acrylic acid present in the film. If the swelling in water is favored by increasing the proportion of PAA it is common to expect a different behavior in oil, as observed in the present work. This result is due to the polarity difference between the two fluids (oil and water) and the high hydrophilicity of PAA, suggesting that starch probably has greater affinity for the SO when compared to PAA.

TPSIM was also applied to evaluate the variation of M_i/M_∞ and the result is presented in Fig. 7. It was possible to observe that M_i/M_∞ was also affected by samples composition. In order to reinforce the applicability of TPSIM to predict the behavior of PAA-S films, in the present work, this method was applied to different data sets. That is, the data set provided by the interpolation was reduced and the comparison between the predicted and experimental points may be observed in Fig. 8. Even with the reduction of the experimental data set, the surfaces generated by TPSIM presented similar behaviors, which corroborates the application of this method for data prediction.

The statistical analysis, ANOVA, was performed to evaluate the data presented in Fig. 8. Thus, the obtained values for the following samples were compared: PAA-S90, PAA-S70, PAA-S60, PAA-S40, PAA-S20 and PAA-S10. Statistical analysis showed that for these samples there was not a significant difference when comparing real and predicted data, which reinforce the TPSIM application in the analysis of PAA and starch films behavior ($p<0.05$).

The analysis of the curves obtained by TPSIM shows that Sw (Fig. 5) and the Mi/M∞ relation (Fig. 7) vary with time. Also, evaluating the effect of time it is possible to observe an oscillation when t tends to 55. This result was already expected when considering the characteristics of the samples, such as anisotropy, morphological differences and inter and intramolecular interactions. All these characteristics are heavily influenced by composition. In fact, the observed oscillations in the behavior of the curves reflect the effect of the variable time in the fluid absorption by the sample, as observed in the TPSIM.

The sine function was applied to fit the Mi/M∞ curves. This function was able to fit the experimental and predicted data, with $R2 > 0.99$. The obtained coefficients (a_i, b_i and c_i) for some compositions of the films are shown in Fig. 9, Fig. 10 and Fig. 11, respectively. Regarding the terms of the sine series: a_i is related to composition and it is associated with the swelling capability of the samples (Fig. 9). The b_i coefficient is a direct multiplier of composition and its values varied from 0 to 0.45, increasing proportionally to the increase of i, while the terms in the series tend to decrease.

The c_i terms, which also contribute to the sum, were negative for some compositions and posi-tive for others, contributing to the oscillatory behavior of the fluid incorporation. The function behavior, as well as the experimental and predicted data, showed the absorption capacity and suggested that fluid loss occurred due to compression of the chains. Thus, this function may be applied as a local model to describe the behavior of SO absorption by PAA-S films. In this context, anisotropic media have different diffusion properties in different directions, as in the case of polymer films. As observed in the morphological analysis presented in this work, the morphology of the samples is strongly affected by composition. This behavior is reflected in the coefficient values of the sine function, which confirms the non-linear behavior of the SO absorption by PAA-S films.

CONCLUSION

PAA-S films were successfully obtained by a microwave. FTIR analyses showed that the functional groups of the polymers were preserved. The morphology of the films was affected by the films composition as evidenced by SEM and AFM analyses. The TPSIM was able to predict the swelling behavior of the films and it was possible to see that the oil absorption ca-pacity of the films was also affected by composition, since the greater swelling degree values were obtained for the films with the highest amounts of starch. This fact suggests that starch has better affinity with SO when compared to PAA, although there was a variation in the data, as seen in the fitted surface, probably, due to the heterogeneities present in the samples.

The sine function was able to fit the data for all compositions (R2 >0,99), because it was able to fit the oscillations that occurred as a function of time.

ACKNOWLEDGEMENTS

This study was financed in part by the Coordenação de Aperfeiçoamento de Pessoal de Nível Superior - Brazil (CAPES) – Finance Code 001. The authors would also like to acknowledge CNPQ for their financial support as well as the Program PICV and PROIC of UFRRJ and UFRRJ/IF for the development of the present work.

REFERENCES

1. Wang P-H, Huang B-S, Horng H-C, Yeh C-C, Chen Y-J (2018) Wound healing. J Chinese Med Assoc 81:94–101.

2. Guo S, DiPietro LA (2010) Factors Affecting Wound Healing. J Dent Res 89:219–229.

3. Lee EJ, Kasper FK, Mikos AG (2013) Biomaterials for tissue engineering. Ann Biomed Eng 42:323–337.

4. Sammartino G, Ehrenfest DMD, Shibli JA, Galindo-Moreno P (2016) Tissue Engineering and Dental Implantology: Biomaterials, New Technologies, and Stem Cells. Biomed Res Int 2016.

5. Henkel J, Woodruff MA, Epari DR, Steck R, Glatt V, Dickinson IC, Choong PFM, Schuetz MA, Hutmacher DW (2013) Bone Regeneration Based on Tissue Engineering Conceptions-A 21st Century Perspective. Bone Res 1:216–248.

6. Y. Abdelaal M, S.I. Makki M, R.A. Sobahi T (2012) Modification and Characterization of Polyacrylic Acid for Metal Ion Recovery. Am J Polym Sci 2:73–78.

7. Villanova JCO, Oréfice RL, Cunha AS (2010) Aplicações farmacêuticas de polímeros. Polimeros 20:51–64.

8. Kadajji VG, Betageri G V. (2011) Water soluble polymers for pharmaceutical applications. Polymers (Basel) 3:1972–2009.

9. Zhu W, Chuah YJ, Wang DA (2018) Bioadhesives for internal medical applications: A review. Acta Biomater 74:1–16.

10. Torres FG, Commeaux S, Troncoso OP (2013) Starch-based biomaterials for wound-dressing applications. Starch/Staerke 65:543–551.

11. Ali Akbari Ghavimi S, Ebrahimzadeh MH, Solati-Hashjin M, Abu Osman NA (2014) Polycaprolactone/starch composite: Fabrication, structure, properties, and applications. J Biomed Mater Res - Part A 103:2482–2498.

12. Xu J, Tan X, Chen L, Li X, Xie F (2019) Starch/microcrystalline cellulose hybrid gels as gastric-floating drug delivery systems. Carbohydr Polym 215:151–159.

13. Qi X, Tester RF (2019) Starch granules as active guest molecules or microorganism delivery

systems. Food Chem 271:182–186.

14. Ghavimi SAA, Ebrahimzadeh MH, Shokrgozar MA, Solati-Hashin M, Osman NAA (2015) Effect of starch content on the biodegradation of polycaprolactone/starch composite for fabricating in situ pore-forming scaffolds. Polym Test 43:94–102.

15. Waghmare VS, Wadke PR, Dyawanapelly S, Deshpande A, Jain R, Dandekar P (2018) Starch based nanofibrous scaffolds for wound healing applications. Bioact Mater 3:255–266.

16. García MC, Aldana AA, Tártara LI, Alovero F, Strumia MC, Manzoa RH, Martinelli M, Jimenez-Kairuz AF (2017) Bioadhesive and biocompatible films as wound dressing materials based on a novel dendronized chitosan loaded with ciprofloxacin. Carbohydr Polym 175:75–86.

17. Majewska I, Gendaszewska-Darmach E (2011) Proangiogenic activity of plant extracts in accelerating wound healing - A new face of old phytomedicines.

18. Venugopal JR, Sridhar S, Ramakrishna S (2014) Electrospun plant-derived natural biomaterials for Tissue engineering. Plant Sci Today 1:151–154.

19. Cardoso CRB, Souza MA, Ferro EAV, Favoreto Jr S, Pena JD (2004) Influence of topical administration of n-3 and n-6 essential and n-9 nonessential fatty acids on the healing of cutaneous wounds. Wound Repair Regen 12:235–243.

20. Ganji F, Vasheghani-Farahani S, Vasheghani-Farahani E (2010) Theoretical description of hydrogel swelling: A review. Iran Polym J 19:375–398.

21. Faul A, Powell MJD (1999) Krylov subspace methods for radial basis function interpolation.

22. Chen X, Li W, Chen J, Rao Y, Yamaguchi Y (2014) A combination of TsHARP and thin plate spline interpolation for spatial sharpening of thermal imagery. Remote Sens 6:2845–2863.

23. Löhndorf M, Melenk JM (2017) On Thin Plate Spline Interpolation. In: International conference on spectral and high order methods ICOSAHOM 2016. Rio de Janeiro, pp 451–466.

24. Marra G, Radice R (2010) Penalised regression splines: Theory and application to medical research. Stat Methods Med Res 19:107–125.

25. Khayyam H, Fakhrhoseini SM, Church JS, Milaini AS, Bab-Hadjashar A, Jazar RN, Naebe M (2017) Predictive modelling and optimization of carbon fiber mechanical properties through high temperature furnace. Appl Therm Eng 125:1539–1554.

26. Guo SN, Yang X, Sun HY (2008) Optimal regularization parameter in approximate TPS interpolation. Proc 7th Int Conf Mach Learn Cybern ICMLC 3:1347–1352.

27. Silva GF, da Silva TG, Gobbi VG, Portela TL, Teixeira BN, Mendonça TS, Thiré RMSM, Oliveira RN, Yaunner RS, Rodrigues Jr JA, Mendonça RH (2019) Swelling degree prediction of polyhydroxybutyrate/chitosan matrices loaded with “Arnica-do-Brasil.” J Appl Polym Sci 136:1–10.

28. Bardajee GR, Hooshyar Z (2013) A novel biocompatible magnetic iron oxide nanoparticles/hydrogel based on poly (acrylic acid) grafted onto starch for controlled drug release. J Polym Res 20.

29. Bin-Dahman OA, Jose J, Al-Harthi MA (2015) Compatibility of poly(acrylic acid)/starch blends. Starch/Staerke 67:1061–1069.

30. Zhang M, Cheng Z, Zhao T, Liu M, Hu M, Li J (2014) Synthesis, characterization, and swelling behaviors of salt-sensitive maize bran-poly(acrylic acid) superabsorbent hydrogel. J Agric Food Chem

62:8867–8874.

31. Sethy PK, Prusty K, Mohapatra P, Swain SK (2019) Nanoclay decorated polyacrylic acid/starch hybrid nanocomposite thin films as packaging materials. Polym Compos 40:229–239.

32. Fazeli M, Keley M, Biazar E (2018) Preparation and characterization of starch-based composite films reinforced by cellulose nanofibers. Int J Biol Macromol 116:272–280.

33. Vebber MC, Aguzzoli C, Beltrami LVR, Fetter G, Crespo JS, Giovanela M (2019) Self-assembled thin films of PAA/PAH/TiO2 for the photooxidation of ibuprofen. Part II: Characterization, sensitization, kinetics and reutilization. Chem Eng J 361:1487–1496.

FIGURES AND TABLES

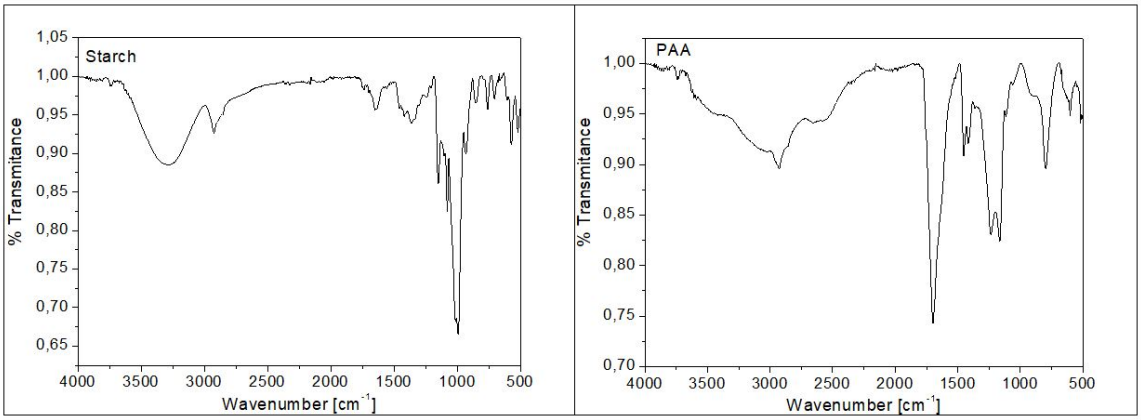

Fig. 1 FTIR spectra of Starch and PAA films.

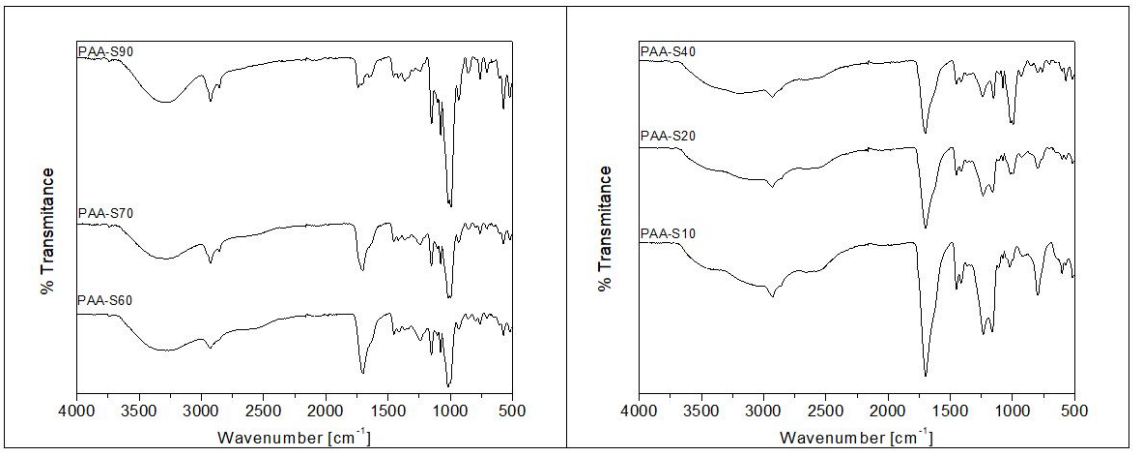

Fig. 2 FTIR of PAA-S films: PAA-S90, PAA-S70, PAA-S60, PAA-S40, PAA-S20 and PAA-S10.

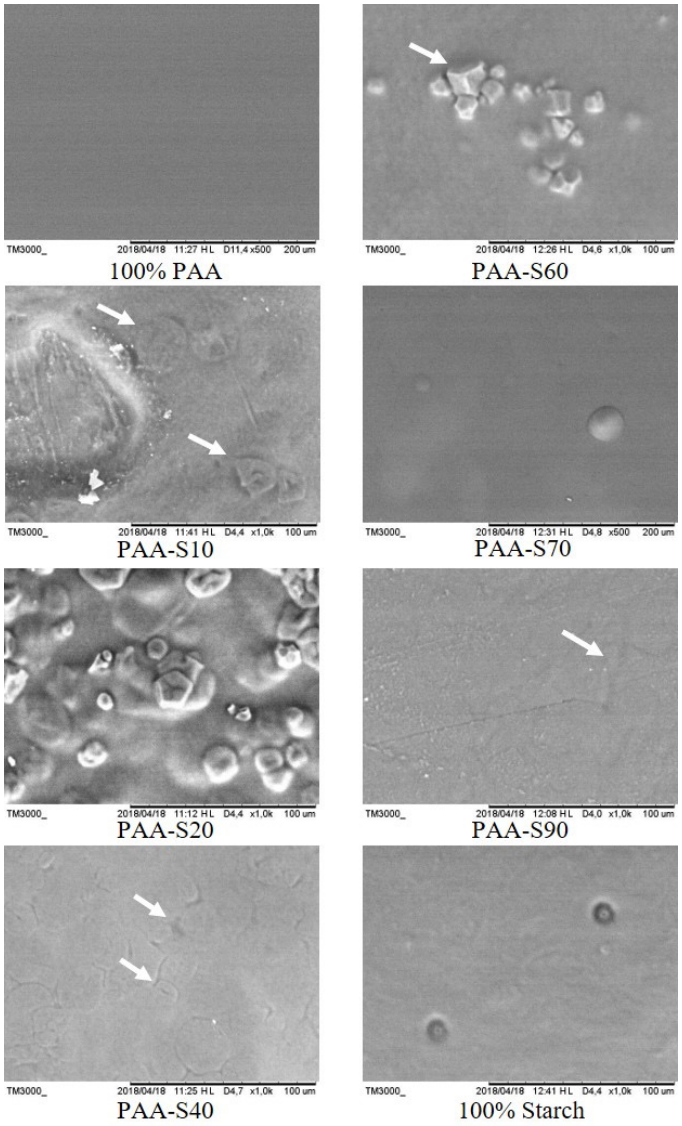

Fig. 3 SEM images of PAA-S films: PAA-S90, PAA-S70, PAA-S60, PAA-S40, PAA-S20 and PAA-S10.

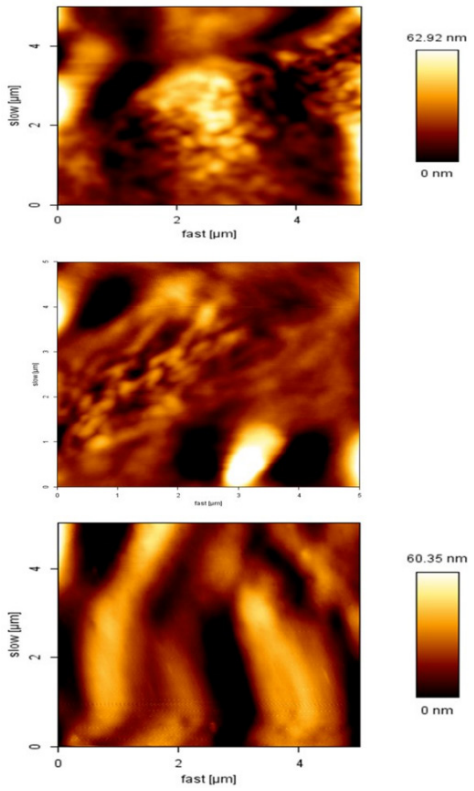

Fig. 4 PAA-S20 (80 wt % and 20 wt % starch) AFM images.

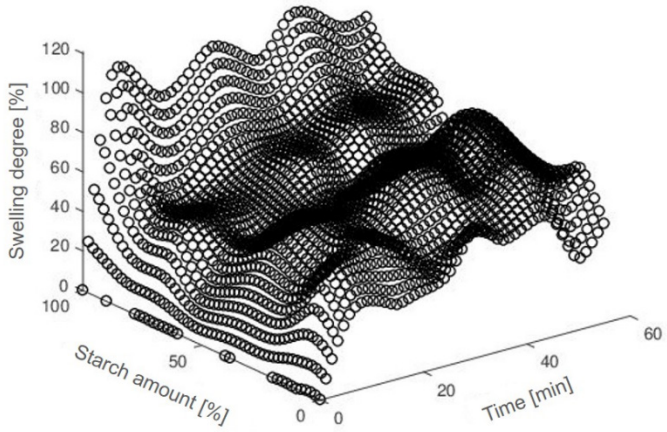

Fig. 5 Swelling degree of the films in SO - TPSIM result.

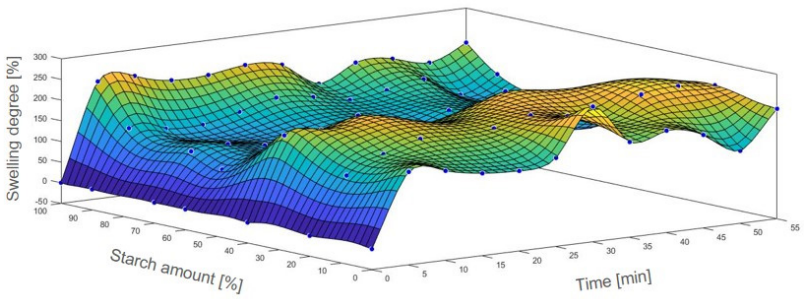

Fig. 6 Swelling degree of the films in SO - predictive surface.

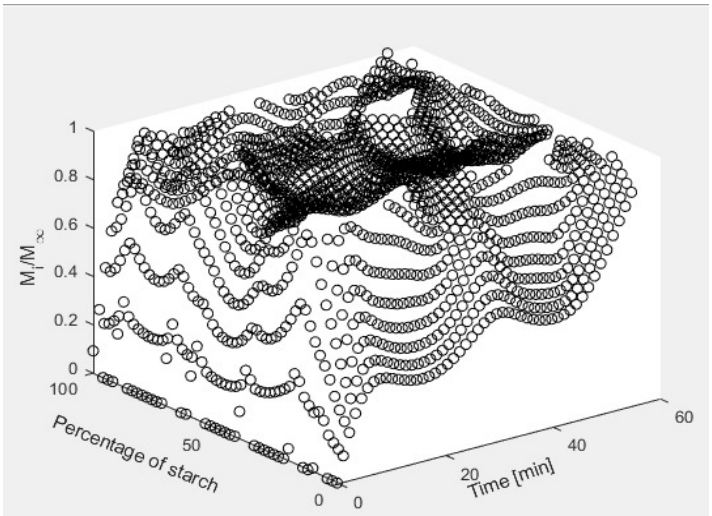

Fig. 7 $M_t/M\infty$ of the films in SO - real and interpolated data.

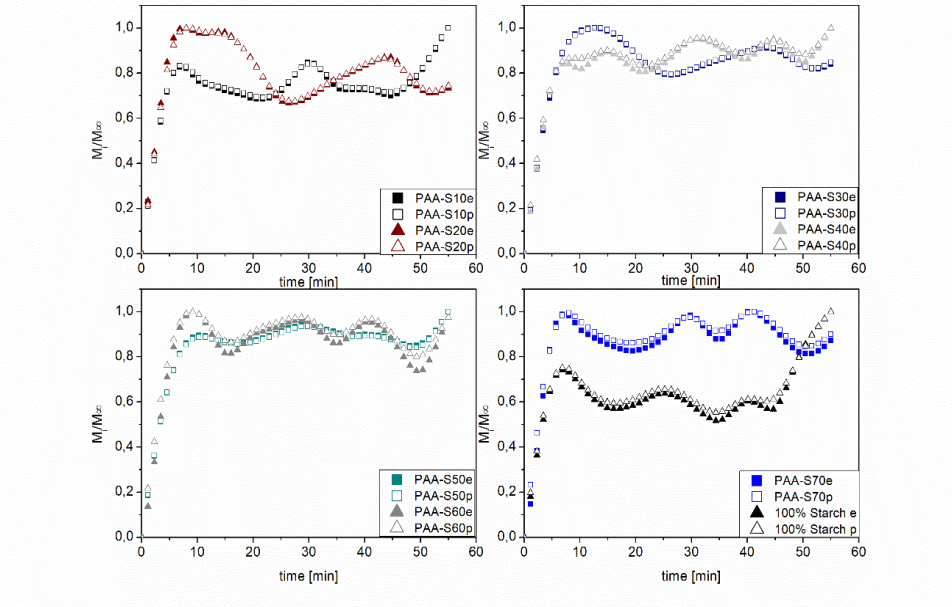

Fig. 8 Predicted (PAA-S10p, PAAS20p, PAA-S30p, PAA-S40p, PAA-S60p, PAA-S70p, 100% starch p) and experimental (PAA-S10e, PAAS20e, PAA-S30e, PAA-S40e, PAA-S60e, PAA-S70e, 100% starch e) data points for different compositions.

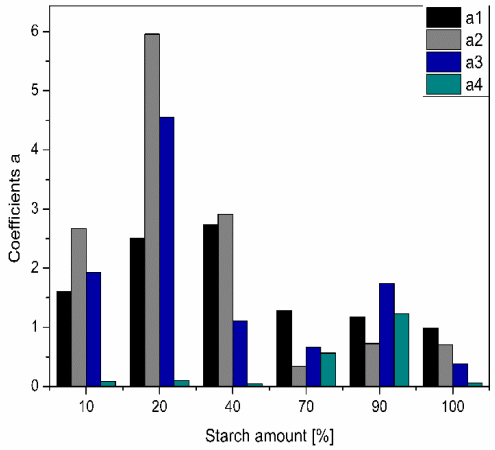

Fig. 9 Values of coefficients ai, obtained by the sine-function fit.

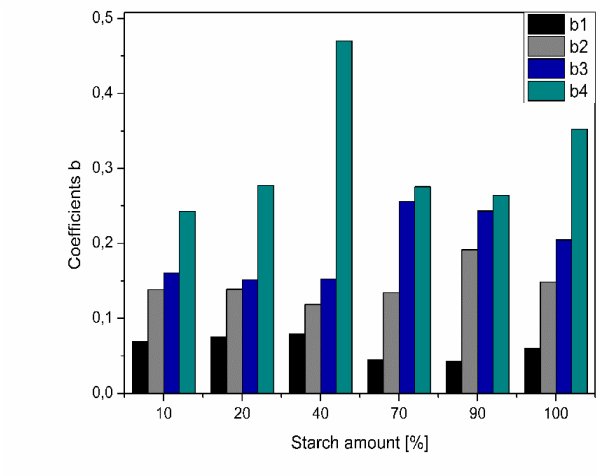

Fig. 10 Values of coefficients bi, obtained by the sine-function.

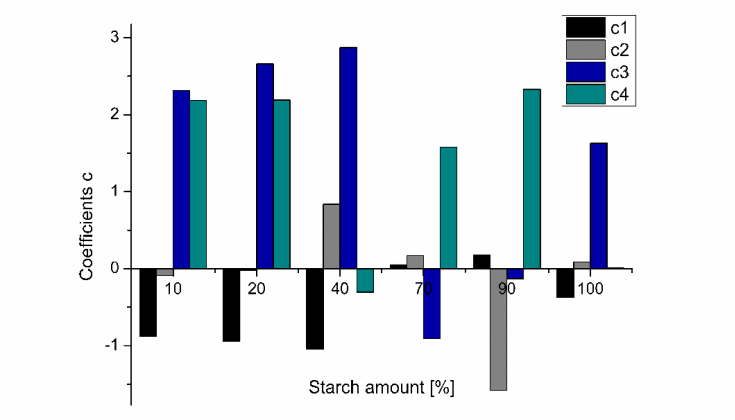

Fig. 11 Values of coefficients ci, obtained by the sine-function.

Band positions starch[cm^{-1}]	Assignments	Band positions PAA [cm^{-1}]	Assignments
3000-3628	-OH stretching of glycosidic group	2900-3600	-OH stretching
2925	CH stretching	2931	CH or CH_2 stretching
1640	-OH bend of absorbed water	1690	C=O stretching
1082-1160	C–O stretching in C–O–H groups	1453	CH_2 deformation
990	C–O stretching in C–O–C bending of α-1,4-glycosidic bond	1414	C-O stretching coupled with O-H

Table 1 FTIR bands of starch and PAA.

Coefficients	Value	Coefficients	Value
p00	-2.207	p31	0.07111
p10	21.22	p22	-0.000379
p01	0.03813	p13	-0.0002123
p20	-17.35	p04	0.0001008
p11	0.9659	p50	0.03999
p02	0.06812	p41	-0.003976
p30	5.699	p32	2.88e-05
p21	-0.438	p23	1.54e-06

p12	0.0101	p14	1.391e-06
p03	-0.004728	p05	-6.454e-07
p40	-0.7992	-	-

Table 2 Coefficients resulting of the polynomial fit p55 presented in Equation (3).

ÍNDICE REMISSIVO

A

B

C

D

E

F

T


Atena
Editora
2020